A Variable Step Size Logarithmic Hyperbolic Cosine Adaptive Filtering-Based Control Scheme for Grid-Tied PV-DSTATCOM to Enhance Power Quality

Markala Karthik
Department of Electrical Engineering
National Institute of Technology Rourkela
Odisha, India
markalakarthikreddy@gmail.com

Venkata Ramana Naik N
Department of Electrical Engineering
National Institute of Technology Rourkela
Odisha, India
nenavathv@nitrkl.ac.in

Anup Kumar Panda
Department of Electrical Engineering
National Institute of Technology Rourkela
Odisha, India
akpanda@nitrkl.ac.in

***Abstract*— A variable step size logarithmic hyperbolic cosine adaptive filtering (VSS-LHCAF)-based control scheme is proposed for a grid-tied multifunctional photovoltaic-distribution static compensator (GTPVD) having single-stage topology for solar energy conversion with maximum power extraction from the PV array. The proposed VSS-LHCAF control scheme is utilized to estimate the fundamental weight components of nonlinear load current accurately in generating the driving pulses for the three-phase two-level voltage source converter (VSC) switches employed in GTPVD, thus enhancing the power quality by mitigating the harmonics produced by nonlinear loads, providing a reactive power compensation, unbalanced load compensation, and maintaining grid currents sinusoidal at unity power factor (UPF). The multifunctional GTPVD system is developed in MATLAB/Simulink. The response of GTPVD is observed under solar irradiance variation and unbalanced loading conditions with a nonlinear load. Further, the proposed control scheme is compared with existing adaptive filtering-based algorithms like least mean square (LMS) and least mean fourth (LMF)-based control schemes, and it is observed that proposed control scheme offers better performance in terms of convergence, oscillations, steady-state error, and grid current total harmonic distortion (THD).**

***Keywords*— Distribution Static Compensator, Least Mean Fourth, Least Mean Square, Photovoltaic, Power Quality, Variable Step Size Logarithmic Hyperbolic Cosine Adaptive Filter.**

I. INTRODUCTION

The rapidly increasing demand for global electrical energy is being met by an exponential increase in renewable energy conversion into electrical energy rather than relying on fossil fuel sources. Solar photovoltaic (PV), a readily available energy source, accounts for a significant share of the various renewable energy sources. The challenges lie in integrating the PV power into the grid while maintaining the power quality (PQ) at grid. The PV power is generally converted into AC power through a voltage source converter (VSC). The VSC functions as a distribution static compensator (DSTATCOM), solving the PQ problems. When VSC performs power conversion and PQ improvement, the effective utilization of solid-state switches in VSC increases. This system is named the grid-tied multifunctional PV-DSTATCOM (GTPVD), which necessitates a control scheme to extract the maximum power from PV arrays, address PQ problems, and inject excess energy into the grid while meeting the load requirement. Several control schemes are presented based on phase-locked loop (PLL) synchronization [1], and others were developed using time and frequency domain analysis. Conventional control schemes necessitate transformations or PLL, which result in delayed responses and are difficult to implement. Several adaptive filtering-based control schemes such as least mean square (LMS) [2], least mean fourth(LMF) [3], and normalized LMS(NLMS) [4] are becoming popular in extracting the fundamental weight components of distorted current as the filter parameters adjust automatically for changing environmental conditions to maintain the system's behavior as intended. In general, it is necessary to build an appropriate cost function specifically for various noise environments. The mean-square error (MSE), which is smooth and tractable mathematically, is frequently employed as a cost function in contexts with gaussian noise. The LMS algorithm is created under the minimum MSE (MMSE) criterion. However, with non-gaussian noises, LMS suffers from considerable performance loss. The LMF method is a higher-order adaptive filter with a fourth-order power optimization. The conventional LMS algorithms have a convergence problem due to drifting [5], whereas the LMF algorithm has stability issues [6]. The accuracy of adaptive filters can be improved by including the hyperbolic cosine function. In order to achieve stabilization in the event of substantial weight errors and to track the steady-state with high accuracy a novel normalization based on the logarithmic hyperbolic cosine function is proposed [7] with variable step size, producing a variable step size logarithmic hyperbolic cosine adaptive filter (VSS-LHCAF)-based control scheme. In terms of stability, steady state error, and resilience against impulsive noise, it excels conventional adaptive filtering algorithms. This paper implemented a VSS-LHCAF-based control scheme to operate a single-stage GTPVD thus enhancing the power quality by mitigating the harmonics produced by nonlinear loads, providing a reactive power compensation, unbalanced load compensation, and maintaining grid currents sinusoidal at unity power factor (UPF).

The paper is organized into five sections. Section II presents GTPVD configuration. Section III presents the overall control scheme for single-stage GTPVD based on the proposed VSS-LHCAF along with extraction of maximum power from PV array. Section IV presents MATLAB/Simulink results for GTPVD under different operating conditions and a comparative assessment of control schemes. The conclusion of this paper is presented in Section V.

II. GTPVD CONFIGURATION

Fig. 1 depicts the configuration of GTPVD. The GTPVD is composed of VSC, PV, dc-link capacitance (C_{dc}), ripple filter (R_{rf} and C_{rf}), and interfacing inductor (L_f). These parameters are designed as illustrated [8]. The ripple filter is

978-1-6654-5566-4/22/$31.00 ©2022 IEEE

used to bypass the high-frequency switching ripples produced by VSC by offering low impedance, and interfacing inductors mitigate current ripples [9].

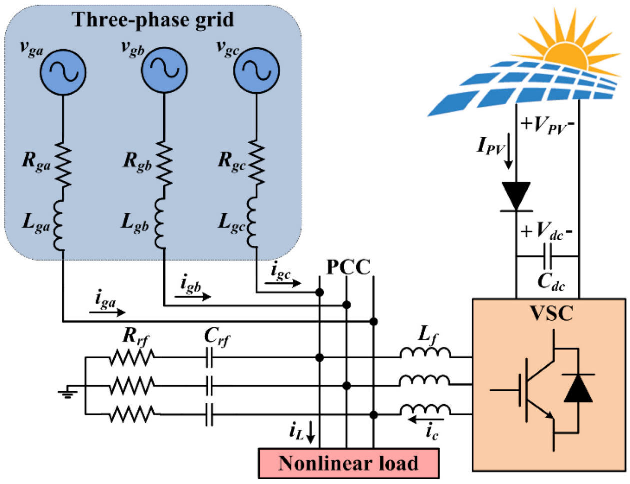

Fig.1. GTPVD configuration

III. Proposed VSS-LHCAF-Based Control Scheme for GTPVD

Minimizing a logarithmic hyperbolic cosine cost function yields VSS-LHCAF control scheme. The LHCAF cost function is smooth to small errors and robust to large errors. As a result, VSS-LHCAF guarantees convergence and stability. The cost function and weight updating equation of the VSS-LHCAF control scheme is given as [7]

$$J(e(i)) = \ln\left\{\cosh\left[\lambda(i)e(i)\right]\right\} \tag{1}$$

$$w(i+1) = w(i) + \mu(i)\tanh\left[\lambda(i)e(i)\right]u(i) \tag{2}$$

where, $e(i)$ is adaptation error, $\lambda(i)$ is a variable scaling factor, and $\mu(i)$ is a variable step size. The values for $\lambda(i)$ and $\mu(i)$ are chosen large initially to obtain a faster convergence rate and then decreased iteratively by using the equations given as

$$\lambda(i) = \alpha_1\lambda(i-1) + \beta_1\exp\left[-\lambda(i-1)\right]\lambda(i-1) \tag{3}$$

$$\mu(i) = \alpha_2\lambda(i-1) + \beta_2\exp\left[-\lambda(i-1)\right]\lambda(i-1) \tag{4}$$

where, $0 < \alpha_1, \alpha_2 < 1$ are the forgetting factors and $\beta_1, \beta_2 > 0$ are the step sizes of the $\lambda(i)$ and $\mu(i)$.

The GTPVD overall control architecture shown in Fig. 2 is divided into five sections as:

A. Generation of PCC Unit Voltage Templates

The phase voltages (v_{ga}, v_{gb}, and v_{gc}) and voltage peak value (V^*_{gt}) at the point of common coupling (PCC) are calculated through sensed line voltages using (5) and (6)

$$\left.\begin{aligned} v_{ga} &= \left(2v_{gab} + v_{gbc}\right)/3 \\ v_{gb} &= \left(-v_{gab} + v_{gbc}\right)/3 \\ v_{gc} &= \left(-2v_{gbc} - v_{gab}\right)/3 \end{aligned}\right\} \tag{5}$$

$$V^*_{gt} = \sqrt{\frac{2}{3}(v_{ga}^2 + v_{gb}^2 + v_{gc}^2)} \tag{6}$$

The in-phase (u_{gpa}, u_{gpb}, and u_{gpc}) and quadrature (u_{gqa}, u_{gqb}, and u_{gqc}) unit voltage templates are estimated as [10]

$$u_{gpa} = \frac{v_{ga}}{V^*_{gt}}; u_{gpb} = \frac{v_{gb}}{V^*_{gt}}; u_{gpc} = \frac{v_{gc}}{V^*_{gt}} \tag{7}$$

$$\left.\begin{aligned} u_{gqa} &= \frac{u_{gpa} - u_{gpb}}{\sqrt{3}} \\ u_{gqb} &= \frac{\sqrt{3}u_{gpa}}{2} + \frac{(u_{gpb} - u_{gpc})}{2\sqrt{3}} \\ u_{gqc} &= \frac{(u_{gpb} - u_{gpc})}{2\sqrt{3}} - \frac{\sqrt{3}u_{gpa}}{2} \end{aligned}\right\} \tag{8}$$

B. Extraction of Maximum Power from PV Array

As power output from PV depends on environmental conditions (temperature and irradiation), numerous maximum power point tracking techniques are available in the literature to operate the PV so as to extract maximum power. Here, an incremental conductance (InC) MPPT [11] is implemented to extract maximum power. The dc-link reference voltage (V^*_{dc}) is considered as PV voltage corresponding to the maximum power point (V_{mpp}).

C. Estimation of Weight Components

The VSS-LHCAF control scheme is used to accurately estimate fundamental active and reactive weight components of nonlinear load current.

The fundamental active weight component of phase 'a' is estimated as

$$w_{pa}(i+1) = w_{pa}(i) + \mu(i)\tanh\left[\lambda(i)e_{pa}(i)\right]u_{gpa}(i) \tag{9}$$

where, $e_{pa}(i)$ is the adaptive error of active weight component at i^{th} instant for phase '*a*'.

$$e_{pa}(i) = i_{La}(i) - u_{gpa}(i)w_{pa}(i) \tag{10}$$

The fundamental reactive weight component of phase 'a' is estimated as

$$w_{qa}(i+1) = w_{qa}(i) + \mu(i)\tanh\left[\lambda(i)e_{qa}(i)\right]u_{gqa}(i) \tag{11}$$

where, $e_{qa}(i)$ is the adaptive error of reactive weight component at i^{th} instant for phase '*a*'.

$$e_{qa}(i) = i_{La}(i) - u_{gqa}(i)w_{qa}(i) \tag{12}$$

Similarly, fundamental active and reactive weight components for phase '*b*' and '*c*' load currents are estimated considering the respective voltage templates and error components.

$$w_{pb}(i+1) = w_{pb}(i) + \mu(i)\tanh\left[\lambda(i)e_{pb}(i)\right]u_{gpb}(i) \tag{13}$$

$$w_{qb}(i+1) = w_{qb}(i) + \mu(i)\tanh\left[\lambda(i)e_{qb}(i)\right]u_{gqb}(i) \tag{14}$$

$$w_{pc}(i+1) = w_{pc}(i) + \mu(i)\tanh\left[\lambda(i)e_{pc}(i)\right]u_{gpc}(i) \tag{15}$$

$$w_{qc}(i+1) = w_{qc}(i) + \mu(i)\tanh\left[\lambda(i)e_{qc}(i)\right]u_{gqc}(i) \tag{16}$$

where, $e_{pb}(i) = i_{Lb}(i) - u_{gpb}(i)w_{pb}(i)$ (17)

$$e_{qb}(i) = i_{Lb}(i) - u_{gqb}(i)w_{qb}(i) \tag{18}$$

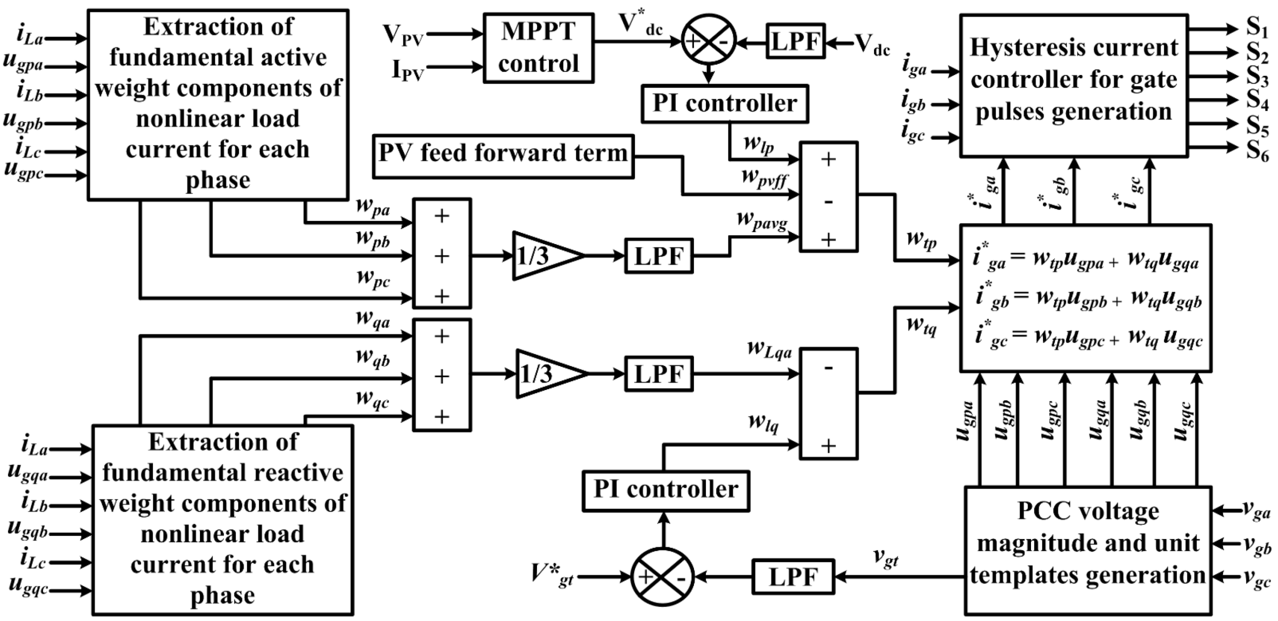

Fig. 2. Control architecture for GTPVD

$$e_{pc}(i) = i_{Lc}(i)-u_{gpc}(i)w_{pc}(i) \quad (19)$$

$$e_{qc}(i) = i_{Lc}(i)-u_{gqc}(i)w_{qc}(i) \quad (20)$$

A PV feedforward component (w_{pvff}) is considered in control scheme to achieve improved dynamic response of grid currents during variation of solar irradiance.

$$w_{pvff} = 2V_{pv}I_{pv}/3V^*_{gt} \quad (21)$$

The active loss component is calculated by implementing a proportional-integral (PI) controller action on dc-link error voltage.

$$w_{lp}(i+1) = w_{lp}(i) + K_{pdc}(V_{dce}(i+1) - V_{dce}(i)) + K_{idc}V_{dce}(i+1)) \quad (22)$$

where, K_{pdc} and K_{idc} are dc-link PI controller parameters and $V_{dce}(i)$ is the error between reference and actual voltages of dc-link.

$$V_{dce}(i) = V^*_{dc}(i)-V_{dc}(i) \quad (23)$$

The reactive loss component is calculated by implementing a proportional-integral (PI) controller action on PCC voltage error.

$$w_{lq}(i+1) = w_{lq}(i) + K_{pac}(V_{gte}(i+1) - V_{gte}(i)) + K_{iac}V_{gte}(i+1)) \quad (24)$$

where, K_{pac} and K_{iac} are PCC voltage PI controller parameters and $V_{gte}(i)$ is the error between reference and actual voltages of PCC.

$$V_{gte}(i) = V^*_{gt}(i)-V_{gt}(i) \quad (25)$$

The total weight of active fundamental components is estimated as

$$w_{tp} = w_{pavg} + w_{lp} - w_{pvff} \quad (26)$$

where, w_{pavg} is the average of fundamental active weight components of three phases.

$$w_{pavg} = (w_{pa} + w_{pb} + w_{pc})/3 \quad (27)$$

The total weight of reactive fundamental components is estimated as

$$w_{tq} = w_{lq} - w_{qavg} \quad (28)$$

where, w_{qavg} is the average of fundamental reactive weight components of three phases.

$$w_{qavg} = (w_{qa} + w_{qb} + w_{qc})/3 \quad (29)$$

D. Estimation of Grid Reference Currents and Generation of Driving Pulses

The grid reference current signals are estimated as

$$i^*_{ga} = w_{tp}u_{gpa} + w_{tq}u_{gqa} \quad (30)$$

$$i^*_{gb} = w_{tp}u_{gpb} + w_{tq}u_{gqb} \quad (31)$$

$$i^*_{gc} = w_{tp}u_{gpc} + w_{tq}u_{gqc} \quad (32)$$

The driving pulses for VSC switches are generated using a hysteresis current controller by passing the error among grid reference currents and sensed grid currents through it.

IV. Results And Discussion

The GTPVD is developed in MATLAB/Simulink. The PV array is designed for 11kW of power for which 20 modules connected in series form a string and 2 such strings are connected in parallel. A nonlinear load of 5kW is considered in the form of a diode bridge rectifier followed by a series R-L load to draw nonlinear current. The response of GTPVD is observed under different operating conditions.

A. Steady State Performance with Balanced Nonlinear load

As depicted in Fig.3 (a) and (b), during steady state condition, PV array is generating 11kW of power, out of which 5kW is delivered to load and the additional power of 6kW is delivered to grid. Despite the fact that load draws distorted currents, grid currents (i_{gabc}) are sinusoidal and these are 180^0 phase opposition with grid voltages(v_{gabc}), indicating that the excess power is being delivered to grid from PV after fulfilling load. The negative sign of grid power (P_g) indicates that the generated PV power is fed to load as well as injecting to grid. The grid reactive power (Q_g) is compensated by compensator to ensure unity power factor (UPF) operation. The dc-link voltage follows its reference value (700 V) throughout operation using MPPT method.

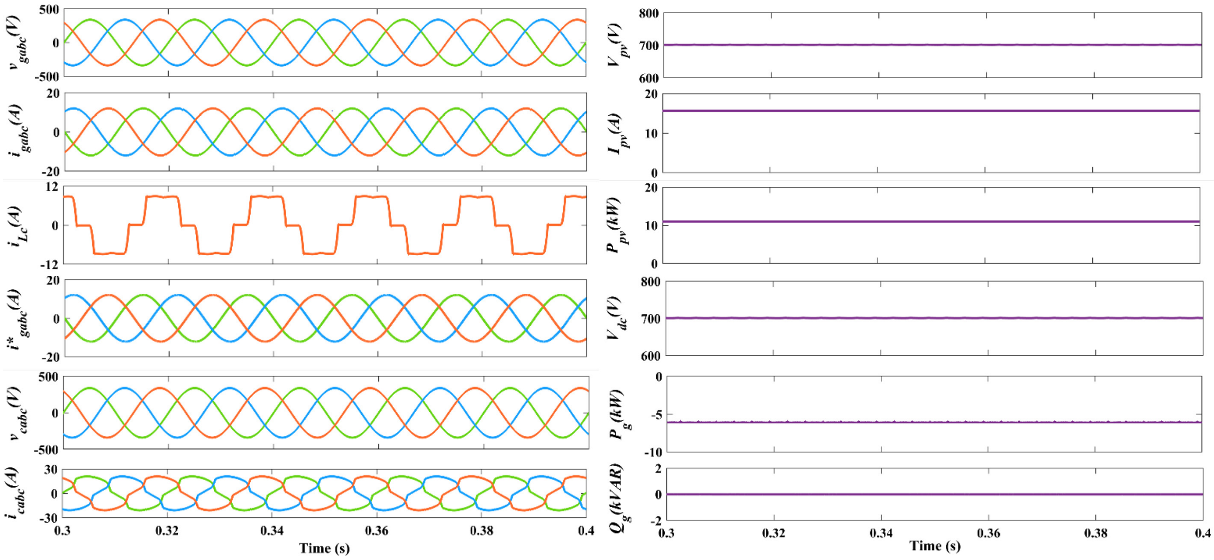

(a) (b)

Fig. 3. Steady state performance of GTPVD with balanced nonlinear load

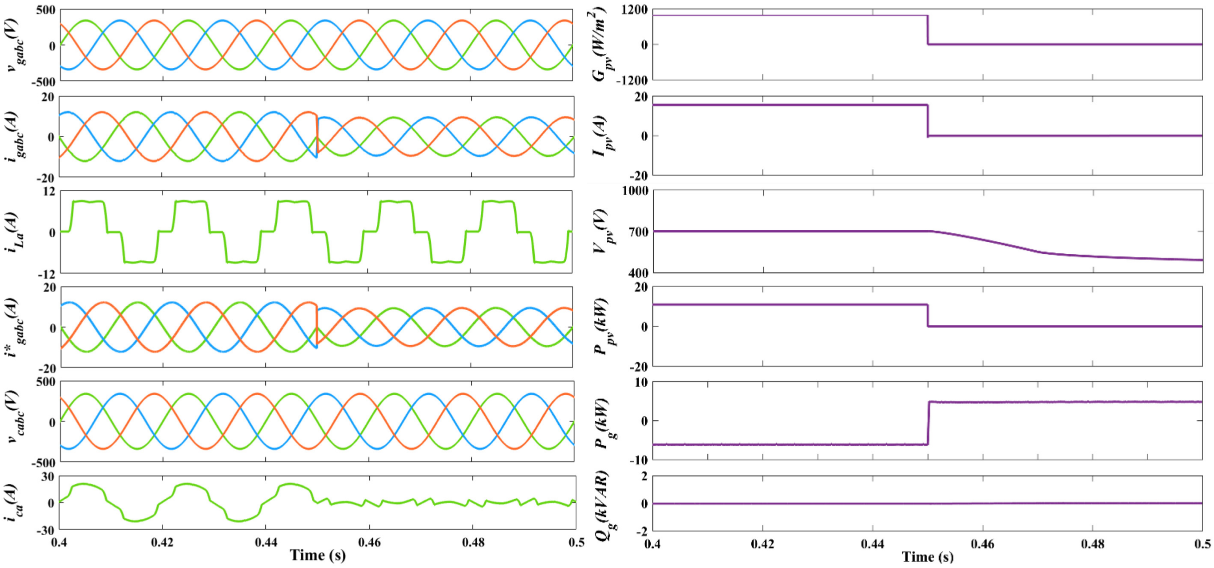

(a) (b)

Fig. 4. Dynamic performance of GTPVD at variable irradiation

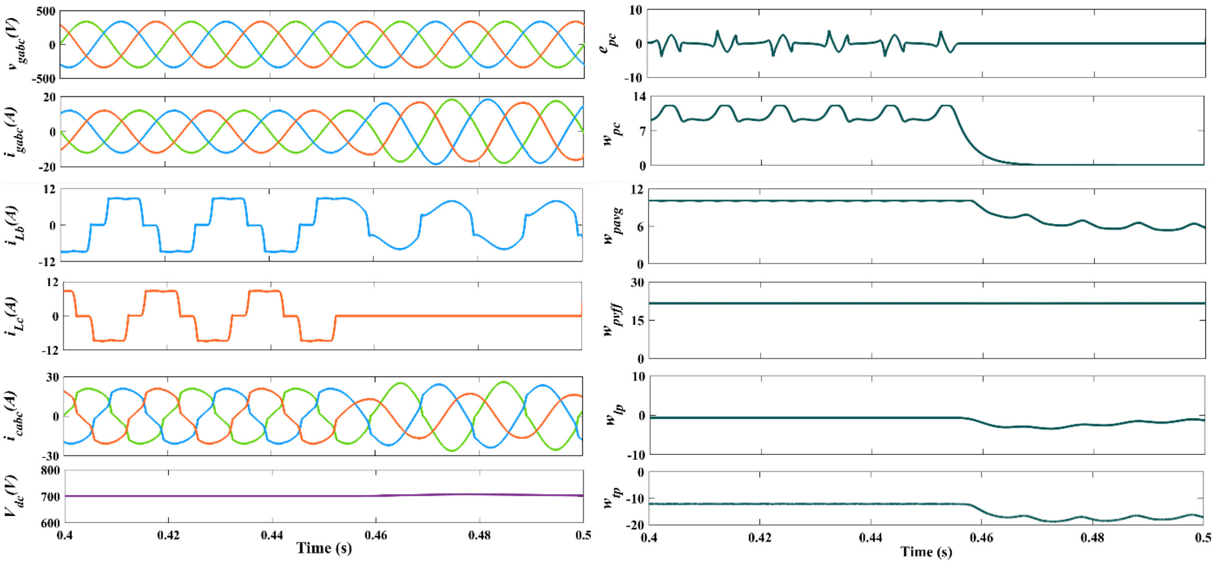

(a) (b)

Fig. 5. Dynamic performance of GTPVD with unbalanced non-linear load

B. *Dynamic Performance at Variable Solar Irradiation*

The dynamic behavior of GTPVD at variable irradiation is depicted in Fig. 4 (a) and (b). The solar irradiation (G_{pv}) is changed to 0 W/m^2 from 1000 W/m^2 at 0.45 s. Before the variation of irradiation, 6kW of PV power is delivered to the grid after fulfilling load (5kW) from 11kW of generated PV power. After changing the solar irradiation, the grid fulfills the load requirement(5kW), during which the VSC continues to provide harmonics mitigation and maintain reactive power as zero. It is observed that the grid currents magnitude is decreased and are in phase with the grid voltages starting from 0.45 s, indicating there is no power to the grid due to the non-availability of PV power and grid is delivering required power to the load.

C. *Dynamic Performance with an Unbalanced Nonlinear Load*

The dynamic performance of GTPVD is shown in Fig. 5 (a) and (b) when GTPVD is connected to an unbalanced nonlinear load. The phase '*c*' of the load is disconnected at 0.45 s to create an unbalanced load. Even if load currents are unbalanced, sinusoidal currents with UPF are maintained at grid but with increased magnitude due to less drawing of power by the unbalanced load and as PV array is adding its power simultaneously in the system. The dc-link voltage (V_{dc}) tracks reference value. The adaptive error active component of phase '*c*' is zero. The weight components (w_{pc}, w_{pavg}, w_{lp}, w_{tp}) are varied and then settled to newer values.

D. *THD Calculation*

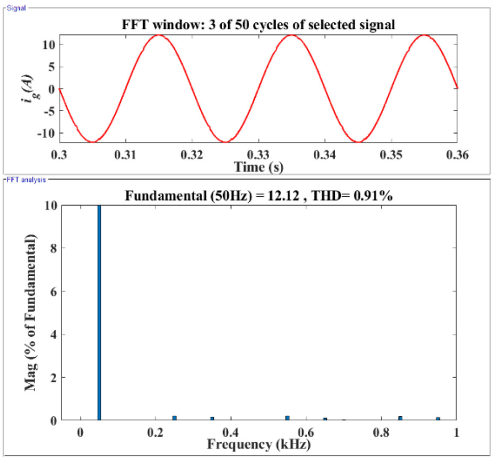

(a)

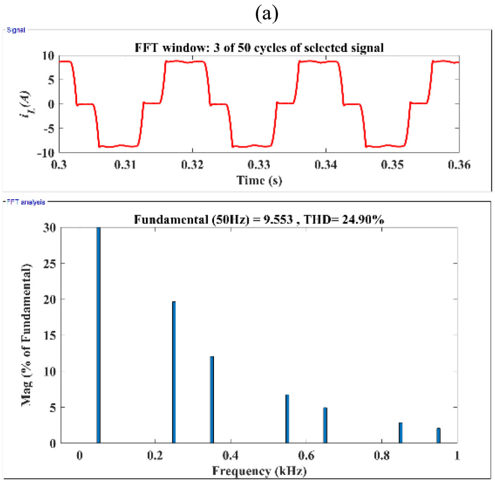

(b)

Fig. 6. (a) THD of grid current, and (b) THD of nonlinear load current

Fig. 6 (a) and (b) shows harmonic spectra of grid current (i_g) and nonlinear load current (i_L). The total harmonic distortion (THD) of 'i_g' is 0.91%, which follows IEEE-519 standard [12] while the THD of 'i_L' is 24.9%.

E. *Comparative Assessment of Control Schemes*

Fig.7. shows average fundamental active weight component (w_{pavg}) estimated by proposed VSS-LHCAF, LMS, and LMF-based control schemes during unbalanced loading condition, which is created by disconnecting phase '*c*' of load from 0.45 s to 0.65 s. A comparative assessment of LMS, LMF, and proposed VSS-LHCAF-based control schemes is provided in Table I under steady state and dynamic conditions. With the proposed VSS-LHCAF-based control scheme, oscillations in 'w_{pavg}' are nearly zero compared to that of LMS and LMF-based control schemes during steady state as well as unbalanced load operating conditions. LMS and LMF control schemes employs a fixed step size, whereas VSS-LHCAF control scheme adjusts step size to achieve faster convergence and less steady state error in estimating the weight components.

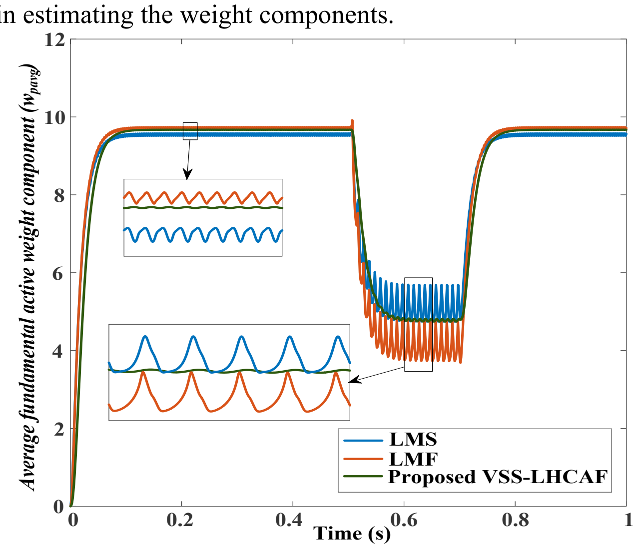

Fig. 7. Estimation of 'w_{pavg}' for proposed VSS-LHCAF, LMS, and LMF-based control schemes

TABLE I. COMPARATIVE ASSESSMENT OF CONTROL SCHEMES

Control Scheme	**Steady state condition**		**Dynamic condition**		
	Oscillations	***Accuracy***	***Oscillations***	***Tracking***	***Deviation***
LMS	High	Poor	More	Moderate	High
LMF	High	Poor	More	Fast	High
Proposed VSS-LHCAF	Very less	Better	Very less	Fast	Less

V. CONCLUSION

A VSS-LHCAF-based control scheme for the GTPVD is proposed which mitigates the harmonics, providing a reactive power compensation, unbalanced compensation, and maintaining grid currents sinusoidal at UPF, thus enhancing PQ while integrating PV power to grid. The response of GTPVD for proposed VSS-LHCAF control scheme is observed by developing GTPVD in MATLAB/Simulink. It is observed that VSS-LHCAF control scheme offers better performance in terms of convergence, oscillations, steady state error, and grid current THD when compared with existing adaptive filtering algorithms such as LMS and LMF-based control schemes.

REFERENCES

[1] K. Sridharan and B. Chitti Babu, "Accurate Phase Detection System Using Modified SGDFT-Based PLL for Three-Phase Grid-Interactive Power Converter During Interharmonic Conditions," *IEEE Trans. Instrum. Meas.*, vol. 71, pp.1-11, Dec 2021.

[2] M. Mangaraj and A. K. Panda, "Sparse LMS algorithm for two-level DSTATCOM," *IET Gener. Transm. Distrib.,* vol. 15, no. 1, pp. 86–96, Jan 2021.

[3] R. K. Agarwal, I. Hussain, and B. Singh, "LMF-based control algorithm for single stage three-phase grid integrated solar PV system," *IEEE Trans. Sustain. Energy*, vol. 7, no. 4, pp. 1379–1387, Oct. 2016.

[4] D. Jaraniya and S. Kumar, "Grid Interactive Charging Station using ZAJO-NLMS Adaptive Filtering Technique with Improved Power Quality for EV Applications," *J. Inst. Eng. Ser. B*, vol. 103, no. 3, pp. 845–857, June 2022.

[5] X. B. Li, Y. Y. Fan, and K. Peng, "A variable step-size LMS adaptive filtering algorithm," *Proc. - 5th Int. Conf. Wirel. Commun. Netw. Mob. Comput. WiCOM 2009*, no. 2, pp. 1–4, Sep 2009.

[6] E. Eweda, "Global stabilization of the least mean fourth algorithm," *IEEE Trans. Signal Process.*, vol. 60, no. 3, pp. 1473–1477, Dec 2011.

[7] S. Wang, W. Wang, K. Xiong, H. H. C. Iu, and C. K. Tse, "Logarithmic Hyperbolic Cosine Adaptive Filter and Its Performance Analysis," *IEEE Trans. Syst. Man, Cybern. Syst.*, vol. 51, no. 4, pp. 2512–2524, Apr 2021.

[8] S. B. Q. Naqvi, S. Kumar, and B. Singh, "Weak Grid Integration of a Single-Stage Solar Energy Conversion System with Power Quality Improvement Features under Varied Operating Conditions," *IEEE Trans. Ind. Appl.*, vol. 57, no. 2, pp. 1303–1313, Jan 2021.

[9] B. Singh, A. Chandra, and K. Al-Haddad, Power Quality Problems and Mitigating Techniques. London, U.K.: Wiley, 2015.

[10] S. Kumar and B. Singh, "Self-Normalized-Estimator-Based Control for Power Management in Residential Grid Synchronized PV-BES Microgrid," *IEEE Trans. Ind. Informatics*, vol. 15, no. 8, pp. 4764–4774, Mar 2019.

[11] J. Mishra, S. Das, D. Kumar, and M. Pattnaik, "Performance Comparison of PO and INC MPPT Algorithm for a Stand-alone PV System," *2019 Innov. Power Adv. Comput. Technol. i-PACT 2019*, no. 1, pp. 1–5, Mar 2019.

[12] IEEE Recommended Practice and Requirements for Harmonic Control in Electric Power Systems, IEEE Std 519-2014, 2014.